Materials Research. 2025; 28: e20240562
DOI: https://doi.org/10.1590/1980-5373-MR-2024-0562

Creep Behavior of Uncoated, Bond-Coated, and Thermal Barrier coated Ti-6Al-4V

Flavio Perpetuo Briguente*[a], *Renata Jesuina Takahashi*[b], *Leonardo Henrique Fazan*[b], *Adriano Gonçalves dos Reis*[c], *Danieli Aparecida Pereira Reis*[b]

[a]*Evonik Corporation, Department of Process Technology and Engineering, Theodore, USA.*
[b]*Universidade Federal de São Paulo, Instituto de Ciência e Tecnologia, São José dos Campos, SP, Brasil.*
[c]*Universidade Estadual Paulista (UNESP), Instituto de Ciência e Tecnologia, Departamento de Engenharia Ambiental, São José dos Campos, SP, Brasil.*

Received: December 07, 2024; Revised: May 01, 2025; Accepted: June 22, 2025

The Ti-6Al-4V alloy is widely used in aerospace components due to its high strength-to-weight ratio and favorable combination of properties, including low density, mechanical strength, corrosion resistance, and creep resistance. However the alloy loses strength and stability above 500°C due to oxidation. To enhance performance and increase its lifespan or working temperature, thermal barrier coat (TBC) is applied. The TBC consists of a substrate, metallic bond coat (BC), thermally grown oxide layer (TGO), and ceramic top coat (TC). The objective of this work was to study the creep behaviour of Ti-6Al-4V alloy without and with BC (NiCoCrAlY) and TBC (NiCoCrAlY + ZrO_2-$YO_{1,5}$) coatings applied by plasma spraying. Creep tests were performed under constant load conditions at a stress of 125 MPa and temperatures of 500, 600, and 700 °C. The creep parameters were determined, and material characterization by optical microscopy. The results showed that the Ti-6Al-4V alloy with BC and TBC exhibited average increases in creep resistance of 77% and 131%, respectively, compared to the uncoated alloy. These coatings resulted in a reduction in the secondary creep rate and an enhancement in creep lifetime. Microstructural analysis revealed that the delamination of the layers increased with the operating temperature.

Keywords: *Ti-6Al-4V alloy, NiCoCrAlY, BC, TBC, Creep.*

1. Introduction

This study aims to conduct a comparative analysis of the creep behavior of Ti-6Al-4V alloy with the application of BC and TBC, applied using the plasma spraying technique. This research is significant due to the necessity of enhancing the creep properties of the alloy at elevated temperatures and reducing oxidation in aggressive environments, such as those encountered in turbine engines.

Titanium alloys are widely utilized in aerospace components due to their high strength-to-weight ratio. Among these, the Ti-6Al-4V alloy is the most commonly used in the aerospace industry, owing to its favorable combination of properties and workability. This alloy is particularly noted for its excellent characteristics, such as low density, as well as superior mechanical strength, corrosion resistance, and creep resistance[1]. Ti-6Al-4V is an α-β alloy that offers a balanced combination of strength, toughness, and high-temperature performance[2,3]. Despite its high melting temperature (≈ 1650 °C), Ti-6Al-4V does not retain satisfactory strength and stability above 500 °C due to oxidation, which leads to the onset of creep and consequently reduces the lifespan of components[4].

Creep is a phenomenon in which a material undergoes slow and continuous plastic deformation over time. It becomes particularly significant when the material is subjected to high temperatures and stress, as is the case for components used in the aerospace industry. The mechanisms of creep are influenced by both stress and temperature, and they can be characterized by the stress exponent and activation energy. Other factors that impact the dominant creep mechanism include the presence of grain boundaries, voids, and interfaces. The primary mechanisms of creep deformation in metallic alloys include: a) atomic transport by diffusion, b) dislocation motion, and c) grain boundary sliding[5-7].

The importance of studying the creep behavior of materials is underscored by the increasing demand for higher operating conditions in structural components developed for the aerospace and energy industries, with the aim of improving efficiency and extending the lifespan of costly components. Energy efficiency can be enhanced by operating turbine engines at progressively higher temperatures, thereby reducing carbon dioxide emissions from aircraft and stationary gas turbines used in power generation plants[8-11].

To mitigate the creep phenomenon, it is essential to understand the mechanisms associated with plastic deformation under high temperature and stress[12,13]. The behavior of metal alloys during plastic deformation at elevated temperatures is complex and varies with thermomechanical processing parameters and operational conditions[14,15]. Numerous studies have been conducted to develop new alloys and, more notably,

*e-mail: danieli.reis@unifesp.br
Associate Editor: Ana Sofia de Oliveira.
Editor-in-Chief: Luiz Antonio Pessan.

to enhance existing commercial alloys[16-26]. In gas turbine engine applications, coatings are employed as a technique to extend the lifetime and increase the operating temperature of titanium alloys. TBCs, in particular, are applied to Ti-6Al-4V alloys to provide thermal and chemical protection for components exposed to aggressive environments at high temperatures[27].

TBCs are multilayer systems composed of a metallic substrate, a BC layer, typically of the MCrAlY type (where M can be Ni, Fe, Co, or combinations thereof), applied to the metallic substrate. Above the BC, there is an intermediate layer of TGO, usually alumina, formed by the oxidation of the BC. The system is completed with a ceramic TC, often consisting of yttria-stabilized zirconia (YSZ), which provides the thermal barrier[1,9,21,22]. The formation of TBC is typically carried out using plasma spraying, specifically air plasma spraying. This technique involves the deposition of powders onto the substrate surface, where the powder particles are fed into a torch or gun and heated to near their melting point. The resulting droplets are then projected onto the surface by a gas stream. Upon impact, the droplets flatten into thin lamellar particles that adhere to the surface, overlap, and solidify, forming the protective coating[23].

TBC and surface treatments have been extensively studied to enhance the creep lifetime of Ti-6Al-4V alloy by providing protection against oxidation and corrosion in components subjected to high temperatures[10,24-43]. These coatings are particularly crucial for components used in the hot sections of gas turbine engine[21]. Studies have demonstrated that Ti-6Al-4V alloy with TBCs exhibits improved mechanical resistance[19,44].

A study on the effect of TBCs and the testing environment (air and nitrogen) on the creep behavior of equiaxial Ti-6Al-4V alloy, at temperatures ranging from 500 to 700 °C, found that the higher the temperature and the lower the applied stress, the greater the thermal barrier efficiency of the TBC for the substrate[10] Researchers also investigated the effect of heat treatment on creep in Ti-6Al-4V alloy, and in the structure exhibiting the highest creep resistance (Widmanstätten), TBC was deposited via plasma spraying. At all temperatures and stresses analyzed, the Widmanstätten + TBC structure demonstrated lower creep rates and longer time to rupture compared to the Widmanstätten structure without the coating[33].

Although mechanical tests indicate that the Widmanstätten microstructure presents the best mechanical properties, the titanium alloy currently used in turbine blades has an equiaxed microstructure. The TBC has been shown to improve the creep life of the Ti-6Al-4V compared to the uncoated alloy; however, there are few studies in the literature that have examined the creep behavior of titanium alloys with BC or TBC. Therefore, this study aims to understand the creep behavior of the equiaxed Ti-6Al-4V alloy with TBC (NiCrAlY and 8YSZ) applied by plasma spraying, as is done commercially.

2. Materials and Method

The Ti-6Al-4V alloy were in the form of cylindrical bars with a length of 1.0 m and a diameter of 12.7 mm. The bar was in the forged and annealed condition at 190°C for 6 hours, followed by air cooling, resulting in an equiaxial microstructure. The chemical composition of the major elements by weight % conforms to the requirements of ASTM B265-10[45]. Chemical analysis was conducted using inductively coupled plasma optical emission spectroscopy (ICP-OES) with an ARL model 3410 instrument. The specimens were prepared for creep tests in accordance with ASTM E139-11[46] as shown in Figure 1.

The coating of the specimens was performed at Rolls-Royce. The chemical composition of the powder used for applying the TC was zirconia (ZrO_2) partially stabilized with 8% by weight of yttria (Y_2O_3), while the metallic powder composition consisted of NiCoCrAlY. The application of both the BC and TBC on Ti-6Al-4V alloy specimens with an equiaxial microstructure was carried out by Rolls-Royce in accordance with the company's procedures for coating turbine blades.

The equiaxial alloy specimens for creep testing were prepared for BC application following these steps: Step 1. The surface of the specimen was blasted using 60-grit aluminum oxide; Step 2. Degreasing was then performed using acetone; Step 3. Masking was applied using high-temperature tape suitable for metallization; Step 4. Finally, to produce a uniform BC layer of 0.127 mm, NiCoCrAlY powder with a particle size of approximately 45 μm was applied via plasma spraying on the substrate (Bond Coat Amdry 995C).

The equiaxial alloy specimens for creep testing were prepared for TC application following the steps described above (steps 1 to 4). Step 5. Subsequently, the stabilized zirconia ceramic powder with 8% by weight of yttria, having a particle size range of approximately 45 μm, was applied via plasma spraying (top coat Metco 204B NS), forming a medium layer of 0.635 mm over the previously applied BC layer.

For both coatings, the process was carried out using a Sulzer Metco Type 9 MB thermal spray equipment, following the

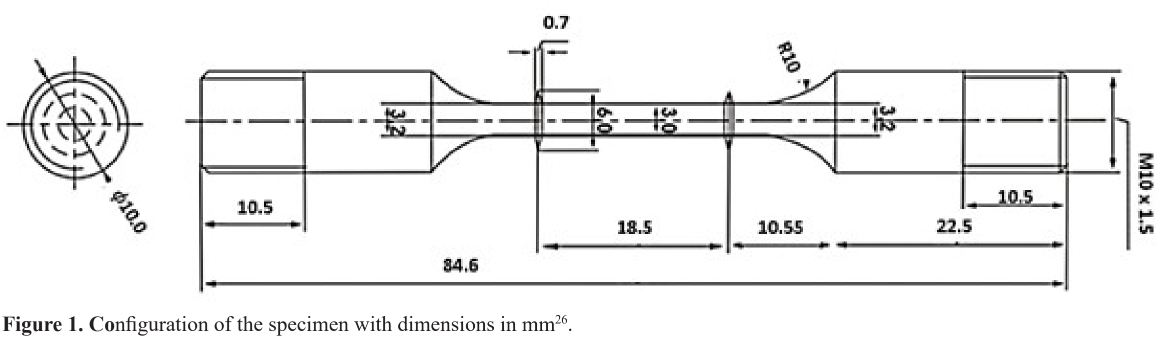

Figure 1. Configuration of the specimen with dimensions in mm[26].

parameters established by Rolls-Royce. The specific plasma spraying process conditions have not been disclosed due to a confidentiality agreement. Figure 2 illustrates the steps involved in the application of both the BC and TC layers on the Ti-6Al-4V alloy specimens with an equiaxial microstructure.

The creep tests were conducted in Mayes furnaces in accordance with the requirements of ASTM E139-11[46]. The tests were performed under constant load mode at a load of 125 MPa and at temperatures of 500, 600, and 700 °C, across three different conditions: Ti-6Al-4V alloy without coating, Ti-6Al-4V alloy with BC (NiCoCrAlY), and Ti-6Al-4V alloy with TBC. The testing conditions were as follows: a) three tests at a stress of 125 MPa at 500 °C; b) nine tests at stresses ranging from 125 MPa to 319 MPa at 600 °C; c) three tests at a stress of 125 MPa at 700 °C. The specimens of the different coatings tested are shown in Figure 3.

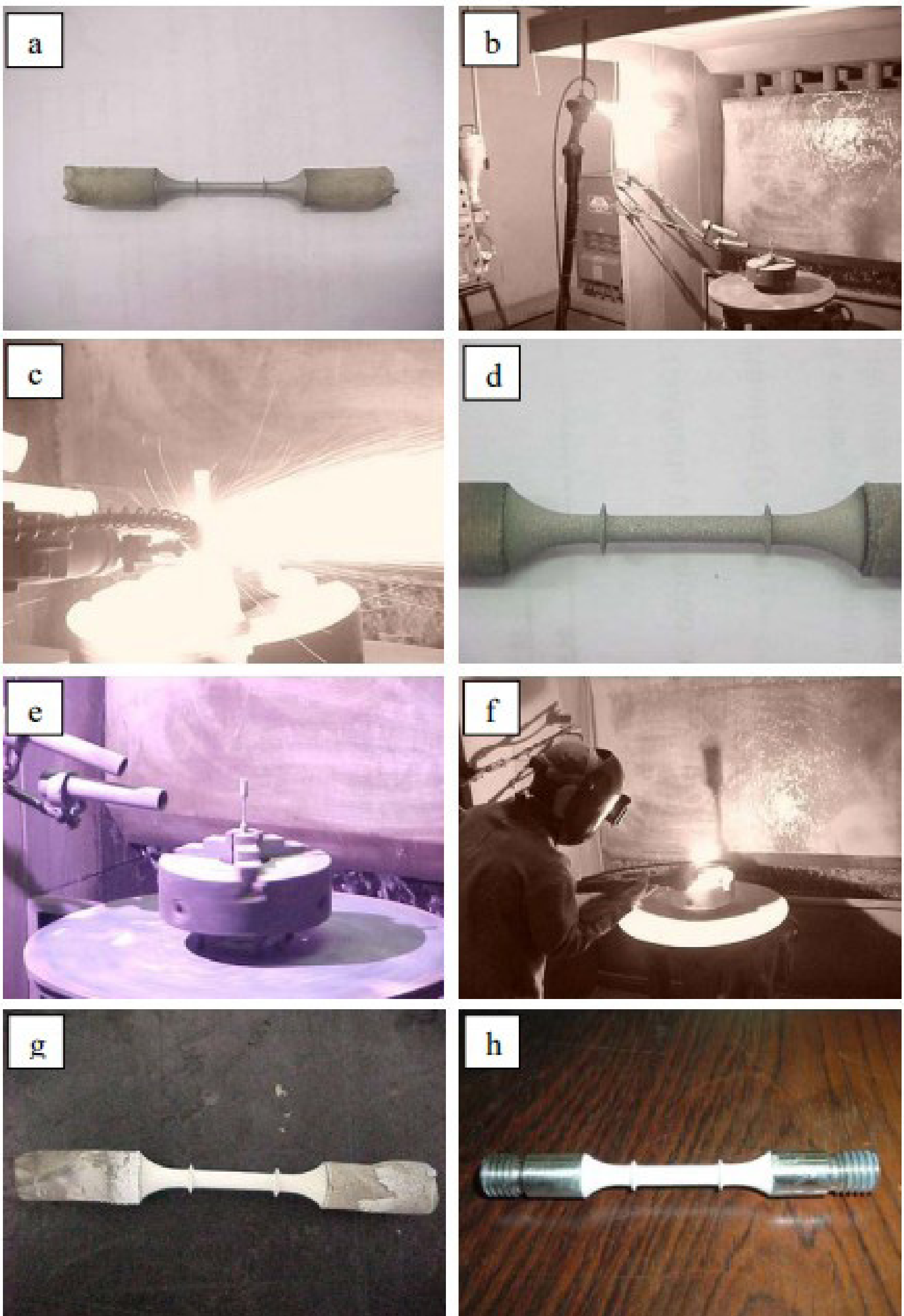

Figure 2. Images of the coating process stages for the specimens in the creep test 26. a) Specimens after Sandblasting; b) Preparation of the equipment; c) Application of the BC layer; d) Specimens with the BC layer; e) Specimens prepared for TC application; f) Application of the TC layer; g) Specimens with the TC layer; h) Specimens covered with the TBC for the creep test.

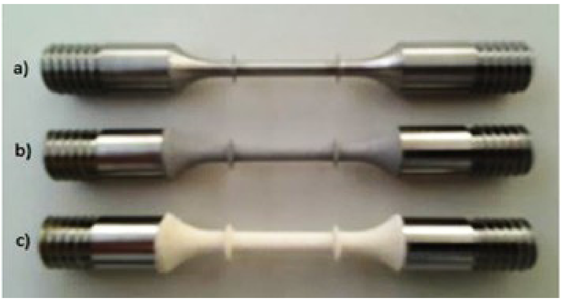

Figure 3. Photographs of the Ti-6Al-4V equiaxial alloy specimens with (a) no coating, (b) BC coating, and (c) TBC coating.

Antares Software was used to collect data on the elongation of the specimens and temperature measurements at predetermined time intervals. A Type Cromel-Alumel thermocouple (AWG24) was employed to measure the temperature. Elongation measurements were obtained using a linear variable differential transformer (LVDT), Schlumberger model D 6.50, with a specification of 53.18 mV/V/mm. The output signal from the LVDT was sent to a controller, which converted the signals into elongation measurements for predefined time intervals, subsequently feeding the data to Antares Software.

Microstructural characterization was performed using optical microscopes: Zeiss model Axioscope A1 BIO and Zeiss model Neophot 3. Sample preparation for optical microscopy involved cutting the specimens after the creep tests in both the transverse and longitudinal directions, using a precision cutter (Buehler, Isomet Low Speed SAW) with a diamond blade and cooling fluid. During the polishing stage, Struers OP-Chem polishing cloth was used with a polishing solution consisting of colloidal silica and H_2O_2. To reveal the microstructure, Kroll's reagent was applied, with the following composition: 5 mL HNO_3, 3 mL HF, and 100 mL distilled water.

Scanning electron microscopy (SEM), using a TESCAN model Vega3, was employed to examine the main characteristics of the fracture surfaces after the creep tests. The microstructural analysis focused on evaluating the variations in microstructure and the characteristics of the fracture surfaces. Sample preparation for SEM involved cleaning the specimens using acetone PA as a cleaning solvent in a Cole Parmer 8890 ultrasound cleaning unit.

The power-law creep equation that describes the creep behavior is presented in Equation 1, where B is the structure-dependent constant and n is the creep stress exponent[47].

$$\acute{Y}_S = B\sigma^n \tag{1}$$

3. Results and Discussion

The chemical composition of the Ti-6Al-4V alloy specimens was as follows: Ti = 89.16%, Al = 6.61%, and V = 4.23% by weight.

The creep data and curves corresponding to the results of the creep tests under 125 MPa stress are presented in Table 1 and Figure 4, respectively. The secondary creep rate refers to the material's resistance to creep, as the majority of the creep lifetime is observed during the secondary stage, where the creep rate remains nearly constant[47]. The results indicate that the equiaxial structure of the titanium alloy with the TBC exhibited the highest creep resistance, with the lowest stationary creep rate and the longest creep lifetime across all applied temperature conditions.

The specimens with BC and TBC demonstrated an average increase in creep resistance of 77% and 131%, respectively, at the three test temperatures, compared to the Ti-6Al-4V alloy without coating. The superior performance of the TBC structure is attributed to the thermal barrier effect of the TC layer, while the enhanced performance of the BC structure is associated with its role as a barrier against oxidation and the diffusion of oxygen into the alloy.

Figure 4 illustrates the effect of temperature on the TBC equiaxial structure. It was observed that as the temperature increased, there was a significant reduction in creep lifetime. This observation is consistent with Norton's Law[47], which states that the resistance to creep decreases as temperature increases, for the same stress conditions.

Figure 5 illustrates the comparison effect of temperature for specimens with (a) no coating, (b) BC, and (c) TBC structures. It was observed that as the temperature increased, there was a significant reduction in creep lifetime for all specimens for the same stress condition of 125 MPa. This observation is consistent with Norton's Law[47], which states that the resistance to creep decreases as temperature increases, for the same stress conditions.

An increase in creep resistance was observed for the specimens with BC and TBC as the temperature increased, in comparison to the specimens without coatings. The ratio of the rupture time for BC and TBC specimens relative to the specimens without coatings is presented in Table 2.

Based on the ratios presented above, it is observed that both coatings act as protective layers on the surface of the Ti-6Al-4V alloy with equiaxial microstructure. The level of protection increased with temperature for the same applied stress. However, superior performance was observed for the TBC compared to the BC, at all working temperatures, which confirms that the TC layer functions effectively as a thermal barrier.

In studies[33] on creep in titanium alloys with TBC, an increase from 1.03 (at 500 ºC) to 2.16 (at 700 ºC) was observed in the ratio between the creep rupture time of the Ti-6Al-4V alloy with a Widmanstätten structure, both with and without TBC. Greater creep resistance was also observed in air-tested Ti-6Al-4V alloy samples with coatings, and the coating efficiency increased with temperature[12]. These studies demonstrate the enhanced efficiency of the TBC as a thermal barrier with increasing working temperature.

The creep mechanisms can be estimated by the values of the stress exponent and the activation energy for creep. The values of the stress exponent (n) and the constant (B) at a temperature of 600 °C can be estimated, as presented in Table 3.

The values of n found in this study range from 3.59 to 3.88, which are consistent with those reported in the literature and support a dislocation creep mechanism for the equiaxial Ti-6Al-4V alloy[8,9,48-52].

According to literature, the creep behavior of Ti-6Al-4V alloy in air was studied, yielding a stress exponent value of 3.4 at a temperature of 600 ºC, with the creep mechanism predominantly associated with the α phase[48]. The value of n equal to 4.12 is consistent with a dislocation creep mechanism for the equiaxed

Table 1. Data from the creep tests at 125 MPa.

T (°C)	Specimen	t_p (h)	$\dot{\varepsilon}_s$ (1/h)	t_f (h)	ε_f (mm/mm)
500	Ti-6Al-4V	16.0	0.0003	427.0	0.1918
	Ti-6Al-4V BC	32.0	0.0002	665.0	0.1726
	Ti-6Al-4V TBC	48.0	0.0001	804.0	0.1735
600	Ti-6Al-4V	0.67	0.0410	5.58	0.4017
	Ti-6Al-4V BC	1.00	0.0222	9.50	0.3769
	Ti-6Al-4V TBC	1.16	0.0118	11.20	0.3378
700	Ti-6Al-4V	0.01	15.084	0.11	0.5569
	Ti-6Al-4V BC	0.02	0.8031	0.21	0.4667
	Ti-6Al-4V TBC	0.02	0.5390	0.32	0.3849

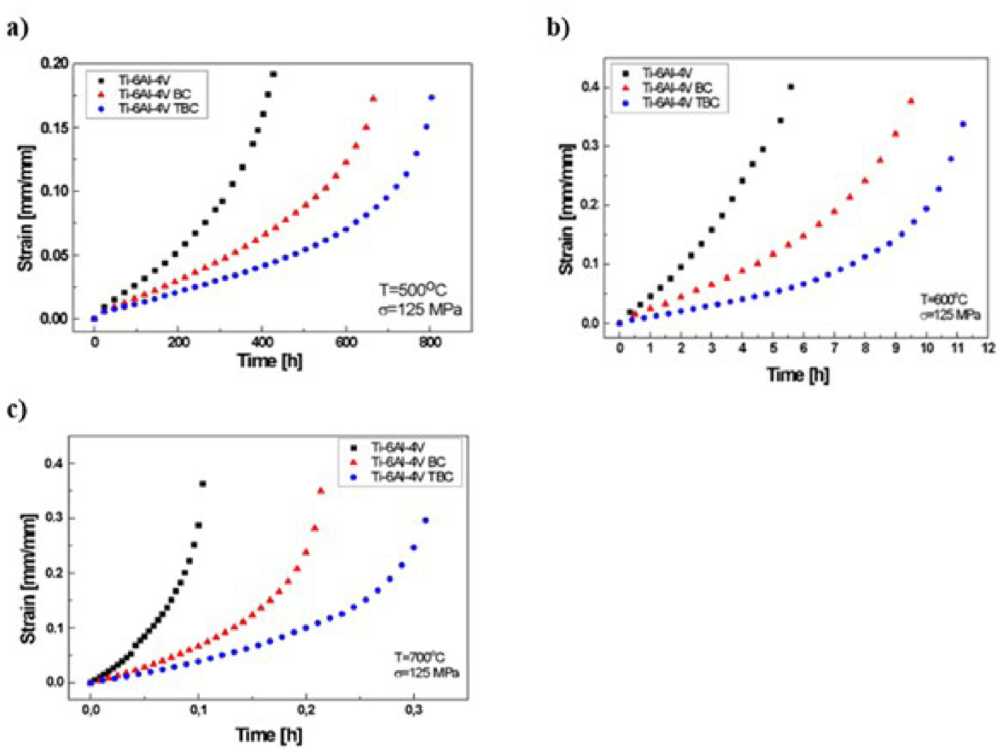

Figure 4. Ti-6Al-4V alloy creep curves with BC and TBC at 125 MPa. (a) 500 °C. (b) 600 °C. (c) 700 °C.

Ti-6Al-4V alloy in air at 600 ºC[49]. Steady-state creep of α/β titanium alloys in the temperature range of 397-552 ºC under constant stress showed stress exponent values of n ranging from 4 to 34[50]. Additionally, values of n at 600 ºC were found to be 3.97 for the equiaxed structure and 5.23 for the Widmanstätten structure[51]. The n values of 4.25 and 5.31 for the Ti-6Al-4V alloy with an equiaxed structure in air and nitrogen atmospheres at 600 ºC were reported, respectively[8]. The stress exponent (n) values found for the various structures at a temperature of 600 ºC were as follows: 3.73 for the bimodal structure, 3.73 for the martensitic structure, 4.91 for the Widmanstätten structure, and 5.63 for the Widmanstätten structure with TBC[19].

Figure 6 presents the micrographs of the cross-section of the Ti-6Al-4V alloy before the creep test, with both the BC and TBC. The optical microscopy analyses after the creep test are shown in Figure 7. The objective of these micrographs was to evaluate the effect of temperature on the delamination process of the coatings. In all micrographs, α-phase (hexagonal close-packed - HCP) grains and dark regions, which define the presence of the β-phase (body-centred cubic), are observed along the grain boundaries.

The micrographs revealed that the Ti-6Al-4V alloy specimens with TBC exhibited greater degradation and delamination of the coating from the substrate as the temperature increased under constant stress (125 MPa). This can be attributed to the enhanced oxidation rate of the material with increasing temperature.

The TBC system is considered compromised when the delamination of the TC layer extends over approximately 20%

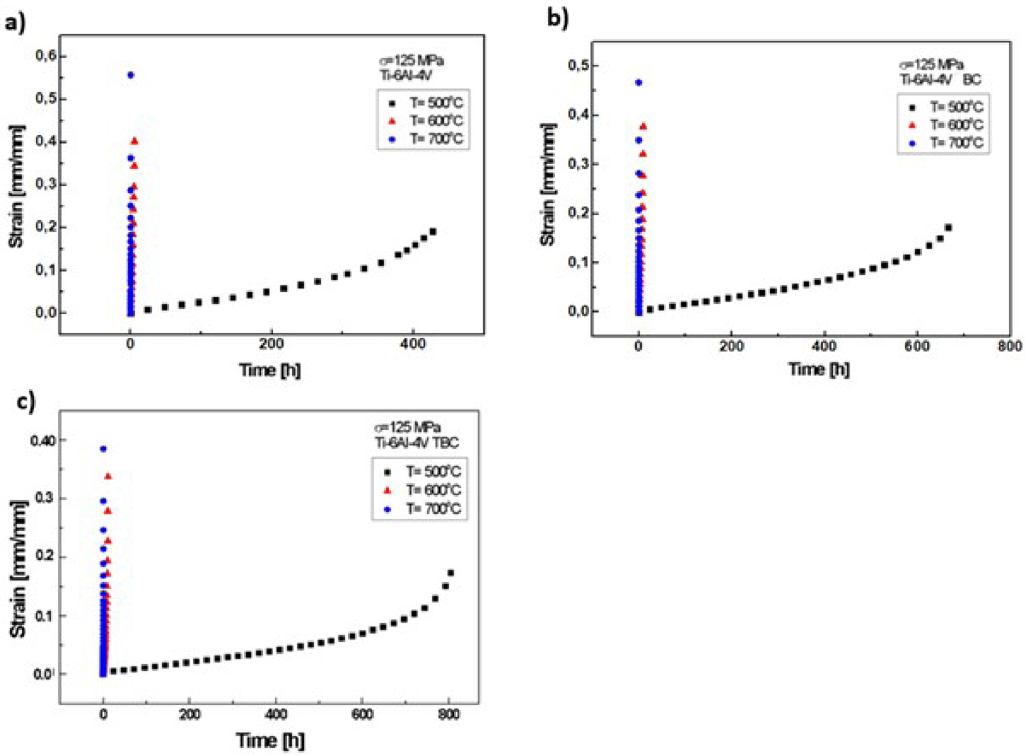

Figure 5. Ti-6Al-4V alloy creep curves at 125 MPa. (a) Ti-6Al-4V uncoated. (b) BC. (c) TBC.

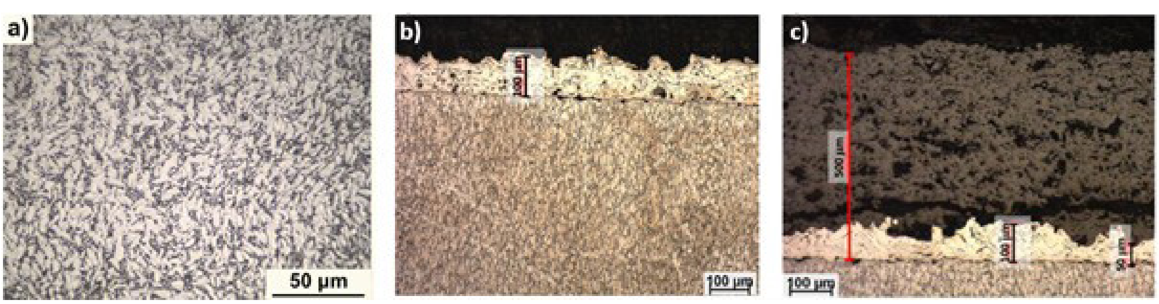

Figure 6. Micrograph of the cross-sectional region of the Ti-6Al-4V alloy before the creep test. a) Ti-6Al-4V no coating. b) BC layer (100 µm); c) TBC layer (BC = 100 / 50 µm and TP = 500 µm).

Table 2. Relationship between the t_f value of the Ti-6Al-4V alloy to the applied coatings.

Temperature	Ratio t_f BC / t_f Ti-Al-4V	Ratio t_f TBC / t_f Ti-Al-4V
500 °C	1.56	1.88
600 °C	1.70	2.01
700 °C	2.05	3.05

Table 3. Stress exponent n and constant B obtained at 600 ºC.

Condition	B	n
Equiaxial	1.19 x 10-09	3.59
Equiaxial BC	2.44 x 10-10	3.79
Equiaxial TBC	8.31 x 10-11	3.88

of the total surface area of the sample, as this significantly reduces its performance as a thermal barrier. The failure of the TBC system occurs due to the delamination of the thermally grown oxide layer on the substrate surface following degradation of the TC layer[53].

Studies aimed at identifying the mechanisms responsible for the delamination of the TC layer primarily focus on the oxidation of the metallic BC. At the interface between the BC and TC layers, oxidation can promote interfacial separation due to the formation of a relatively thick and brittle TGO layer, predominantly composed of Al_2O_3. In TBC systems where the bonding and surface layers do not vary in composition and/or structure, the thickness of the TGO layer correlates well with the likelihood of delamination of the TC layer during thermal cycling[53].

The delamination process of the TBC system is closely related to the applied thermal cycles and working stresses, and is further influenced by the presence of pores and cracks resulting from the manufacturing process. Delamination of the TBC is typically initiated by the failure of the TC layer, which detaches from the BC layer due to the growth of the TGO layer. Once the TC layer detaches, the surface temperature of the BC layer and the substrate alloy increases significantly, accelerating the oxidation kinetics and leading to further delamination of the metal coat[52].

The micrographs of the Ti-6Al-4V alloy with TBC show almost complete detachment of the TC layer, followed by significant delamination of the BC layer at 700 ºC. The preservation of these layers is notably improved with a reduction in the working temperature, as observed in the micrographs from the tests conducted at 500 ºC. Thus, the primary function of the TBC system is to provide a thermal barrier and protect the alloy from oxidation, thereby increasing its lifetime.

Grain size plays an important role and can affect creep behavior. The larger the grain size, the higher the resistance to creep, as the sliding mechanism at the grain boundaries becomes more pronounced. The grain size of the titanium alloy before the creep test is shown in Figure 6a, with an average grain size of approximately 20.60 µm. The deposition processing temperatures of the coatings nor the creep testing temperature conditions did not alter the microstructure of the titanium alloy, as can be observed by comparing the microstructure of Figures 6 and 7.

Fractographic analyses revealed the main characteristics of the fracture surfaces after the creep tests. The fractographic results aimed to evaluate the effect of temperature and coating type under all test conditions of temperature and stress. The phenomena of restriction and the development of microcavities were observed, with ductile fracture mechanisms prevailing in all cases. Figure 8 shows the fractographic analyses of the Ti-6Al-4V alloy with TBC after the creep tests at 125 MPa at

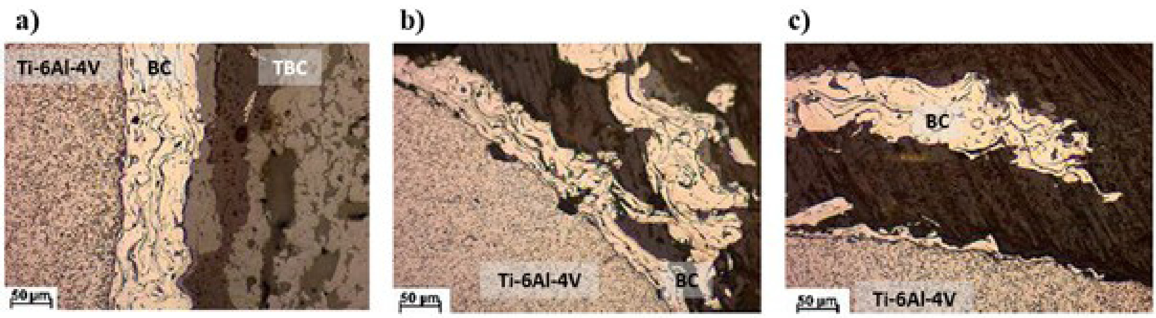

Figure 7. Micrograph of the cross-sectional region of the Ti-6Al-4V alloy after the creep tests at 125 MPa. (a) 500 °C. (b) 600 °C. (c) 700 °C.

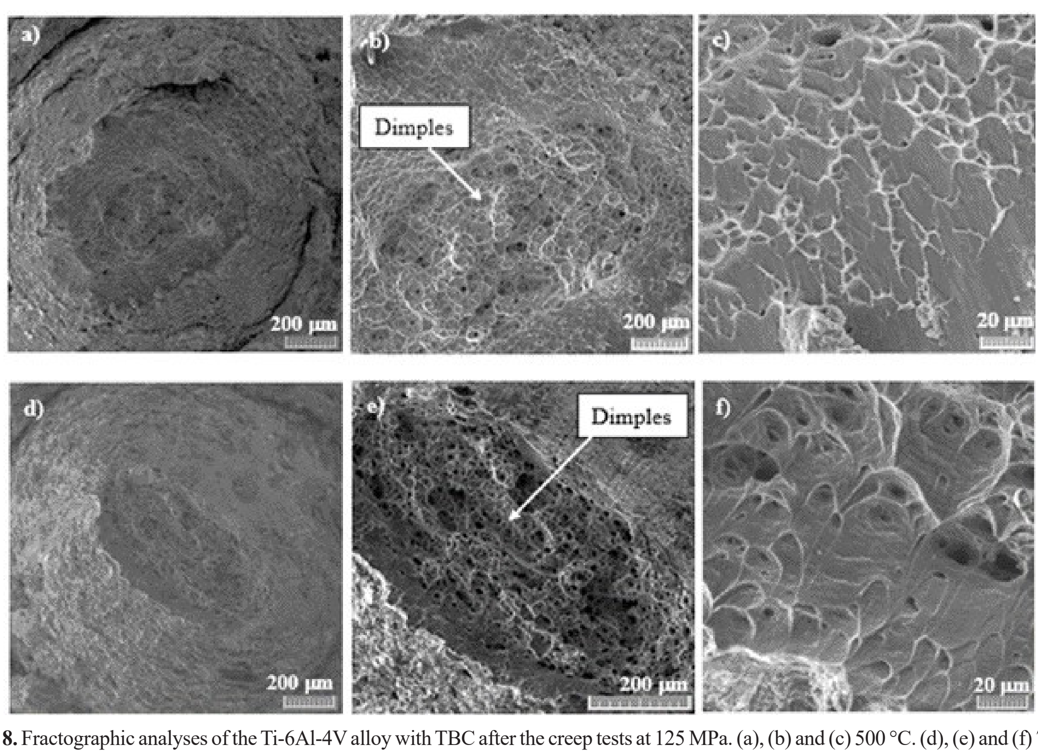

Figure 8. Fractographic analyses of the Ti-6Al-4V alloy with TBC after the creep tests at 125 MPa. (a), (b) and (c) 500 °C. (d), (e) and (f) 700 °C.

500 °C and 700 °C. The central region of the fracture surface at 500 ºC exhibited a uniform structure with equiaxially shaped, shallow dimples. At 600 ºC, the central region of the fracture surface displayed voids and alveolar membranes, while at 700 ºC, deeper changes were observed in the surface, attributed to the higher temperature, oxidation mechanisms, and surface area reduction due to restriction. The micro-mechanisms were similar across all conditions when analyzed at the point of fracture by scanning electron microscopy. Surface coatings did not alter the type of fracture observed after creep; their effect was limited to an increase in fracture time or creep lifetime for the structures with both BC and TBC.

4. Conclusion

The study of creep behaviour of Ti-6Al-4V alloy with BC (NiCoCrAlY) and with TBC (NiCoCrAlY + ZrO_2 – 8% by weight of Y_2O_3) under a constant stress of 125 MPa at temperatures of 500, 600, and 700 ºC led to the following conclusions:

- Samples of the alloy with equiaxed structure, coated with TBC and BC, exhibited higher creep resistance compared to the uncoated equiaxed alloy tested in air. Both TBC and BC demonstrated effectiveness under the tested temperature and load conditions, providing protection against oxidation.
- At temperatures of 500 and 700 ºC and a stress of 125 MPa, the equiaxed TBC structure exhibited superior creep resistance, characterized by longer primary creep time (t_p) and creep life (t_f), and a lower steady-state creep rate (ε), followed by the performance of the equiaxed BC alloy. In these tests, the steady-state creep rates for the uncoated samples were consistently higher.
- The thermal barrier efficiency of both coatings improved with increasing temperature compared to the uncoated alloy. The efficiency of the TBC was greater than that of the BC, due to the significantly lower thermal conductivity of the TC layer.
- For all test conditions, the steady-state creep rate, as well as the primary, secondary, and tertiary creep times, could be described by Norton's power law equations. The stress exponent (n) values ranged from 3.59 to 3.88. The indicator is in agreement with values reported in the literature and are consistent with a dislocation scaling creep mechanism for the equiaxial Ti-6Al-4V alloy.
- Fractographic analyses revealed that the predominant mechanism for all test conditions was characterized by the formation and coalescence of microcavities with varying shapes and sizes. These cavities were wavy in regions of discontinuities, such as inclusions, and possibly at points involving dislocation stacking, where localized stresses induced the formation of voids as a means of relieving local stress. The ductile fracture mechanism predominated under all conditions. The size and shape of the dimples or alveolar structures were determined by the number and distribution of nucleated microcavities and the internal stresses present in the material.
- The failure of the BC is associated with the oxidation process under high stress and temperature conditions. The failure of the TBC system was attributed to the propagation of cracks driven by the oxidation of the BC layer and the stresses applied during the tests.

5. Acknowledgments

This study was supported by Brazilian funding agencies CAPES (Coordination for the Improvement of Higher Education Personnel), CNPq (National Council for Scientific and Technological Development), FINEP (Funding Agency for Studies and Projects), FAPESP (Research and Innovation Support Foundation of Sao Paulo), ITA and Rolls-Royce.

6. References

1. Evans HE. Oxidation failure of TBC systems: an assessment of mechanisms. Surf Coat Tech. 2011;206(7):1512-21. http://doi.org/10.1016/j.surfcoat.2011.05.053.
2. Jiang J, Zhang S, Tao X, Peng D, Yao M, Yi C, et al. Creep behavior of Ti–6Al–4V fabricated by electron beam directed energy deposition. Mater Sci Eng A. 2023;886:145653. http://doi.org/10.1016/j.msea.2023.145653.
3. Hijazi F, Roy B, Srinivasan D, Jayaram V, Kumar P. Non-uniform mechanical behaviour of uniaxially rolled Ti–6Al–4V with micro-texture regions. Mater Sci Eng A. 2023;869:144813. http://doi.org/10.1016/j.msea.2023.144813.
4. Li W, Yan L, Karnati S, Liou F, Newkirk J, Taminger KMB, et al. Ti-Fe intermetallics analysis and control in joining titanium alloy and stainless steel by laser metal deposition. J Mater Process Technol. 2017;242:39-48. http://doi.org/10.1016/j.jmatprotec.2016.11.010.
5. Borges GO, Barboza MJR, Reis DAP. Mathematical modeling applying ν concept and θ projection to creep of Ti-6Al-4V alloy. Mater Res. 2023;26(Suppl 1):e20220555. http://doi.org/10.1590/1980-5373-mr-2022-0555.
6. Fang X, Liu Y, Shao Y, Xu H, Yang F. Forging temperature effects on crack tip creep behaviour of hot hammer forged Ti-6Al-4V alloy. Adv Mater Sci Eng. 2023;2023:4414502. http://doi.org/10.1155/2023/4414502.
7. Pellicotte J, Hossain MA, Egan AG, Mills MJ, Stewart CM. Rapid screening of creep resistance in additive manufactured Ti-6Al-4V alloy. Mater Sci Eng A. 2024;913:146999. http://doi.org/10.1016/j.msea.2024.146999.
8. Funatani K. Emerging technology in surface modification of light metals. Surf Coat Tech. 2000;133-134:264-72. http://doi.org/10.1016/S0257-8972(00)00940-3.
9. Levi CG. Emerging materials and processes for thermal barrier systems. Curr Opin Solid State Mater Sci. 2004;8(1):77-91. http://doi.org/10.1016/j.cossms.2004.03.009.
10. Reis DAP. Efeito do recobrimento cerâmico e da atmosfera de ensaio na fluência de liga metálica refratária de titânio [thesis]. São José dos Campos: Instituto Nacional de Pesquisas Espaciais; 2005.
11. Schulz U, Leyens C, Fritscher K, Peters M, Saruhan-Brings B, Lavigne O, et al. Some recent trends in research and technology of advanced thermal barrier coatings. Aerosp Sci Technol. 2003;7(1):73-80. http://doi.org/10.1016/S1270-9638(02)00003-2.
12. Reis DAP, Moura C No, Silva CRM, Barboza MJR, Piorino F No. Effect of coating on the creep behavior of the Ti–6Al–4V alloy. Mater Sci Eng A. 2008;486(1-2):421-6. http://doi.org/10.1016/j.msea.2007.09.024.
13. Boyer R. An overview on the use of titanium in the aerospace industry. Mater Sci Eng A. 1996;213(1-2):103-14. http://doi.org/10.1016/0921-5093(96)10233-1.
14. Guo FA, Trannoy N, Gerday D. An application of scanning thermal microscopy: analysis of the thermal properties of plasma-sprayed yttria-stabilized zirconia thermal barrier

coating. J Eur Ceram Soc. 2005;5(7):1159-66. http://doi.org/10.1016/j.jeurceramsoc.2004.04.026.
15. Balazic M, Kopac J, Jackson MJ, Ahmed W. Review: titanium and titanium alloy applications in medicine. IJNBM. 2007;1(1):3-34. http://doi.org/10.1504/IJNBM.2007.016517.
16. Huo J, Sun D, Wu H, Wang W, Xue L. Multi-axis low-cycle creep/fatigue life prediction of high-pressure turbine blades based on a new critical plane damage parameter. Eng Fail Anal. 2019;106:104159. http://doi.org/10.1016/j.engfailanal.2019.104159.
17. Viespoli LM, Bressan S, Itoh T, Hiyoshi N, Prashanth KG, Berto F. Creep and high temperature fatigue performance of as build selective laser melted Ti-based 6Al-4V titanium alloy. Eng Fail Anal. 2020;111:104477. http://doi.org/10.1016/j.engfailanal.2020.104477.
18. Almeida GFC, Arbex AA, Oliveira HVD, Domingues NS, Vatavuk J, Reis DAP, et al. Influence of thermal oxidation on the creep behavior of Ti-6Al-4V alloy. Mater Res. 2023;26(Suppl. 1):e20220521. http://doi.org/10.1590/1980-5373-mr-2022-0521.
19. Freitas FF, Briguente FP, Reis AG, Vasconcelos G, Reis DAP. Investigation on the microstructure and creep behavior of laser remelted thermal barrier coating. Surf Coat Tech. 2019;369:257-64. http://doi.org/10.1016/j.surfcoat.2019.04.068.
20. Doleker K, Odabaş O, Ozgurluk Y, Askerov K, Karaoglanli A. Effect of high temperature oxidation on Inconel 718 and Inconel 718/YSZ/Gd2Zr2O7. Mater Res Express. 2019;6(8):086456. http://doi.org/10.1088/2053-1591/ab26d8.
21. Bakan E, Vaßen R. Ceramic top coats of plasma-sprayed thermal barrier coatings: materials, processes, and properties. J Therm Spray Technol. 2017;26(6):992-1010. http://doi.org/10.1007/s11666-017-0597-7.
22. Rajendran R. Gas turbine coatings: an overview. Eng Fail Anal. 2012;26:355-69. http://doi.org/10.1016/j.engfailanal.2012.07.007.
23. Lima CC, Trevisan R. Aspersão térmica: fundamentos e aplicações. 2. ed. São Paulo: Artliber; 2007.
24. Sahoo R, Jha BB, Sahoo TK. Effect of microstructure on the creep properties of Ti–6Al–4V alloys: an analysis. Trans Indian Inst Met. 2018;71(7):1573-82. http://doi.org/10.1007/s12666-018-1292-1.
25. Briguente L, Briguente F, Reis DAP, Moura C, Resende FA. Avaliação do comportamento em fluência da liga Ti-6Al-4V com estrutura martensítica e equiaxial a 600°C. Tecnol Metal Mater Min. 2013;10(4):324-8. http://doi.org/10.4322/tmm.2013.042.
26. Reis DAP, Silva CRM, Nono MCA, Barboza MJR, Piorino F No, Perez EAC. Plasma-sprayed coatings for oxidation protection on creep of the Ti–6Al–4V alloy. Mater High Temp. 2005;22(3):449-52. http://doi.org/10.3184/096034005782744227.
27. Almeida DS, Piorino F No, Henriques VAR, Assis JMK, Gonçalves PAR, Takahashi RJ, et al. Study of non-transformable t′-YSZ by addition of niobia for TBC application. Coatings. 2024;14(3):249. http://doi.org/10.3390/coatings14030249.
28. Takahashi RJ, Assis JMK, Reis DAP. Microstructural characterization of zirconia co-doped with yttria and niobia by laser deposition on Ti-6Al-4V as a thermal barrier for application in turbines. SAE Tech Pap Ser. 2018;1:36-0332. http://doi.org/10.4271/2018-36-0332.
29. Takahashi RJ, Assis JMK, Riva R, Oliveira AC, Reis DAP. Caracterização microestrutural da camada de NiCrAlY sobre Ti-6Al-4V processado por laser de Yb:fibra. Tecnol Metal Mater Min. 2022;19:e2776. http://doi.org/10.4322/2176-1523.20222776.
30. Freitas FE, Briguente FP, Reis AG, Vasconcelos G, Reis DAP. Investigation on the microstructure and creep behavior of laser remelted thermal barrier coating. Surf Coat Tech. 2019;369:257-64. http://doi.org/10.1016/j.surfcoat.2019.04.068.
31. Takahashi RJ, Assis JMK, Piorino F No, Reis DAP. Thermal conductivity study of ZrO2-YO1.5-NbO2.5 TBC. J Mater Res Technol. 2022;19:4932-8. http://doi.org/10.1016/j.jmrt.2022.07.037.
32. Reis AG, Reis DAP, Moura C No, Barboza MJR, Silva CRM, Piorino F No, et al. Influence of laser treatment on the creep of the Ti-6Al-4V alloy. Metall Mater Trans, A Phys Metall Mater Sci. 2011;42(10):3031-4. http://doi.org/10.1007/s11661-011-0834-5.
33. Briguente LAN, Oñoro J, Briguente FP, Resende FA, Reis JL, Reis DAP, et al. The influence of laser nitriding on creep behavior of Ti-4Al-4V alloy with widmanstätten microstructure. Metals. 2019;9(2):1-10.
34. Takahashi RJ, Assis JMK, Piorino F No, Reis DAP. Heat treatment for TGO growth on NiCrAlY for TBC application. Mater Res Express. 2020;6(12):126442. http://doi.org/10.1088/2053-1591/ab6778.
35. Briguente F, Briguente LAN, Reis DAP, et al. Comparative study of creep resistance of a Ti-6Al-4V alloy with metallic and ceramic coatings. Mater Sci Forum. 2014;802:472-6. http://doi.org/10.4028/www.scientific.net/MSF.802.472.
36. Ozgurluk Y, Karaoglanli AC, Ahlatci H. Comparison of calcium–magnesium-alumina-silicate (CMAS) resistance behavior of produced with electron beam physical vapor deposition (EB-PVD) method YSZ and Gd2Zr2O7/YSZ thermal barrier coatings systems. Vacuum. 2021;194:110576. http://doi.org/10.1016/j.vacuum.2021.110576.
37. Karaoglanli AC, Ozgurluk Y, Doleker KM. Comparison of microstructure and oxidation behavior of CoNiCrAlY coatings produced by APS, SSAPS, D-gun HVOF and CGDS techniques. Vacuum. 2020;180:109609. http://doi.org/10.1016/j.vacuum.2020.109609.
38. Ozgurluk Y, Doleker KM, Ozkan D, Ahlatci H, Karaoglanli AC. Cyclic hot corrosion failure behaviors of EB-PVD TBC systems in the presence of sulfate and vanadate molten salts. Coatings. 2019;9(3):166. http://doi.org/10.3390/coatings9030166.
39. Kaplan M, Uyaner M, Ozgurluk Y, Doleker KM, Karaoglanli AC. Evaluation of hot corrosion behavior of APS and HVOF sprayed thermal barrier coatings (TBCs) exposed to molten Na_2SO_4+ V_2O_5 salt at 1000 °C. In: Öchsner A, Altenbach H, editors. Engineering design applications New York: Springer; 2019. p. 441-59. http://doi.org/10.1007/978-3-319-79005-3_28.
40. Ozgurluk Y, Doleker KM, Ahlatci H, Karaoglanli AC. Investigation of calcium–magnesium-alumino-silicate (CMAS) resistance and hot corrosion behavior of YSZ and La2Zr2O7/ YSZ thermal barrier coatings (TBCs) produced with CGDS method. Surf Coat Tech. 2021;411:126969. http://doi.org/10.1016/j.surfcoat.2021.126969.
41. Ozgurluk Y. Investigation of oxidation and hot corrosion behavior of molybdenum coatings produced by high-velocity oxy-fuel coating method. Surf Coat Tech. 2022;444:128641. http://doi.org/10.1016/j.surfcoat.2022.128641.
42. Doleker KM, Ozgurluk Y, Kahraman Y, Karaoglanli AC. Oxidation and hot corrosion resistance of HVOF/EB-PVD termal barrier coating system. Surf Coat Tech. 2021;409:126862. http://doi.org/10.1016/j.surfcoat.2021.126862.
43. Doleker K, Karaoglanli A, Ozgurluk Y, Kobayashi A. Performance of single YSZ, Gd2Zr2O7 and double-layered YSZ/Gd2Zr2O7 thermal barrier coatings in isothermal oxidation test conditions. Vacuum. 2020;177:109401. http://doi.org/10.1016/j.vacuum.2020.109401.
44. Freitas FE, Reis AG, Reis DAP. Comportamento em fluência da liga Ti6Al4V com recobrimento como forma de barreira térmica depositado por aspersão térmica a plasma. In: 73º Congresso Anual da ABM; 2018; São Paulo. Anais. São Paulo: Associação Brasileira de Metalurgia, Minerais e Mineração; 2018. p. 397-406.
45. ASTM: American Society for Testing and Materials. ASTM B265: standard specification for titanium and titanium alloy strip, sheet, and plate. West Conshohocken, PA: ASTM International; 2010.
46. ASTM: American Society for Testing and Materials. ASTM E139: standard test methods for conducting creep, creep-rupture, and stress-rupture tests of metallic materials. West Conshohocken, PA: ASTM International; 2018. http://doi.org/10.1520/E0139-11R18.
47. Evans RW, Wilshire B. Introduction to creep. London: The Institute of Materials; 1993.

48. Warren J, Hsiung LM, Wadley HNG. High temperature deformation behavior of physical vapor deposited Ti6Al-4V. Acta Metall Mater. 1995;43(7):2773-87. http://doi.org/10.1016/0956-7151(94)00464-S.
49. Barboza MJR, Perez EAC, Medeiros MM, Reis DAP, Nono MCA, Piorino F No, et al. Creep behavior of Ti–6Al–4V and a comparison with titanium matrix composites. Mater Sci Eng A. 2006;428(1-2):319-26. http://doi.org/10.1016/j.msea.2006.05.089.
50. Evans WJ, Harrison GF. Power law steady state creep in α/β titanium alloys. J Mater Sci. 1983;18(11):3449-55. http://doi.org/10.1007/BF00544173.
51. Perez EAC. Influência da microestrutura no comportamento em fluência da liga Ti-6Al-4V [dissertation]. Lorena: Faculdade de Engenharia Química de Lorena; 2004.
52. Seo D, Ogawa K, Nakao Y, Miura H, Shoji T. Influence of high-temperature creep stress on growth of thermally grown oxide in thermal barrier coatings. Surf Coat Tech. 2009;203(14):1979-83. http://doi.org/10.1016/j.surfcoat.2009.01.029.
53. Ajdelsztajn L, Hulbert D, Mukherjee A, Schoenung JM. Creep deformation mechanism of cryomilled NiCrAlY bond coat material. Surf Coat Tech. 2007;201(24):9462-7. http://doi.org/10.1016/j.surfcoat.2007.03.054.

Data Availability

The entire dataset that supports the results of this study has been published within the article itself.